Semicond. Sci. Technol. **14** (1999) R17–R25. Printed in the UK PII: S0268-1242(99)97788-X

TOPICAL REVIEW

Quantum-well capture and interwell transport in semiconductor active layers

R Paiella, G Hunziker and K J Vahala

Department of Applied Physics, Mail Stop 128-95, California Institute of Technology, Pasadena, CA 91125, USA

Received 23 September 1998, accepted for publication 29 January 1999

Abstract. The dynamics of electrons and holes in multiquantum-well semiconductor gain media involves several different transport processes, such as diffusion and drift across the barrier region, as well as capture and escape transitions between the bound and the unbound states of the quantum wells. In addition to their fundamental interest, these processes are important because of their implications for the dynamic properties of multiquantum-well lasers and optical amplifiers. Experimentally, they have been studied with several time-domain optical techniques having (sub)picosecond resolution and, more recently, with frequency-domain techniques based on laser modulation measurements. This article gives a brief review of the work done in this area and then presents in detail a frequency-domain approach, four-wave mixing spectroscopy in semiconductor optical amplifiers, to investigate intrinsic capture and interwell equilibration. This technique allows one to extend the device modulation frequency to several hundreds of gigahertz, thus providing the required time resolution, and can be configured to isolate and directly study the transport process of interest.

1. Introduction

The electrical carriers injected into a semiconductor multiquantum-well (MQW) structure are eventually captured into the bound states of the quantum wells (QWs), through a combination of several transport processes. These include classical diffusion and drift across the barrier region, energy relaxation within the band of unconfined states overlaying the barriers' band edges and 'intrinsic' capture into a quantum-confined state, typically mediated by the interaction with a phonon or with another carrier. All of these processes are of significant importance from a fundamental viewpoint, as well as for their implications in the realm of electronic and optoelectronic devices. Therefore they have attracted considerable attention in recent years, within the general context of ultrafast spectroscopy of semiconductor microstructures [1].

Historically, the initial theoretical investigations of the QW capture process [2–9] described it as arising from phonon-assisted intersubband transitions between the 3D states delocalized across the barrier region and the quasi-2D states of the QWs. A remarkable result of these early studies was the prediction of an oscillatory dependence of the capture rate on the QW width. The large body of experimental work that followed [10–26], based on several different techniques, found measured values for the capture lifetime varying over a wide range, from a fraction to tens of picoseconds, depending on the experimental conditions. Similarly, the predicted oscillations with well width were only observed under appropriate conditions [10, 18, 21], most notably in the low carrier density regime, where the lifetime broadening of the delocalized single-particle states is small.

More recently, the interest in the capture problem has been driven by the understanding of its relevance to the dynamic properties of (M)QW lasers [27–36]. In this context, the regime of interest is that of high carrier densities, as provided by the electrical injection, in which case the theoretical description based on unbound states that are completely delocalized across the barrier region becomes inappropriate. Instead, the unconfined carriers are more properly described as semiclassical wavepackets, and a complete analysis of their dynamics should include real-space transport processes such as drift and diffusion. Furthermore, carrier–carrier scattering also significantly contributes to the overall capture rate in this regime. From a device physics standpoint, a debate arose regarding whether the high-speed properties of (M)QW lasers are mainly affected by the transport across the barrier or by the intrinsic capture in the QW states [28–31].

In this article we will review the work done in the past decade to clarify the nature of the capture and interwell transport dynamics in MQW structures and to measure the relevant time constants. A large fraction of the experimental work in this area has relied on ultrafast time-domain techniques, providing the (sub)picosecond resolution required to accurately study the intrinsic capture process.

On the other hand, to study the impact of transport processes on the properties of high-speed (M)QW lasers, frequency-domain techniques, such as modulation response measurements, are appealing, because their results can be more directly related to the modulation dynamics of these devices. In particular, in the final section of the article, we will describe in detail two experiments based on four-wave mixing in semiconductor optical amplifiers and specifically designed to study intrinsic capture and interwell equilibration in the frequency domain. As will be shown, the use of this technique allows one to extend the modulation frequency to hundreds of gigahertz, thus providing the equivalent time resolution required to directly study these processes.

2. Historical survey

A schematic representation of the carrier transport dynamics considered in this work is given in figure 1. As shown there, in MQW active layers electrons and holes are transported into the QW bound states (the states providing the optical gain in these devices) through a combination of electrical injection into the separate confinement region, drift and diffusion across the barriers and intrinsic capture into the QWs. The efficiency of this transport process is commonly quantified with a phenomenological capture lifetime, whose definition, however, varies considerably in different works.

Typically, this time constant is introduced via some rate equation model, and its exact meaning is then strongly dependent on the details of the model. For instance, one may consider a simple picture in which the capture current into a QW is proportional to the overall number of unbound carriers; the proportionality constant is then an effective inverse capture lifetime that includes all of the transport processes mentioned above. Vice versa, one may formulate a more involved model in which drift and diffusion are treated explicitly and introduce a phenomenological capture lifetime describing the quantum transitions only. Furthermore, even if we focus our attention on such an intrinsic (or 'local') capture lifetime, which will be denoted by τ_{cap} in the following, its definition is somewhat dependent on the assumptions that one makes regarding the nature of the unbound carriers. Finally, it should be noted that the lifetime computed in most theoretical works (i.e. the inverse transition rate from an unbound to a bound state of the QW, averaged over the carrier distribution) is not necessarily the appropriate quantity to be used in a small-signal rate equation model.

These considerations are important to keep in mind when discussing the large body of work in this area. Indeed, the large discrepancy in the quoted experimental values of τ_{cap} can at least partly be ascribed to the lack of agreement among the models used to interpret the data.

2.1. The intrinsic capture lifetime

Following early investigations based on a classical scattering model [37, 38], the concept of carrier capture as due to quantum-mechanical transitions into the bound states of a QW was first developed in a 1986 article by Brum and Bastard [2]. In this work, the authors used the Born approximation to compute the LO phonon assisted capture

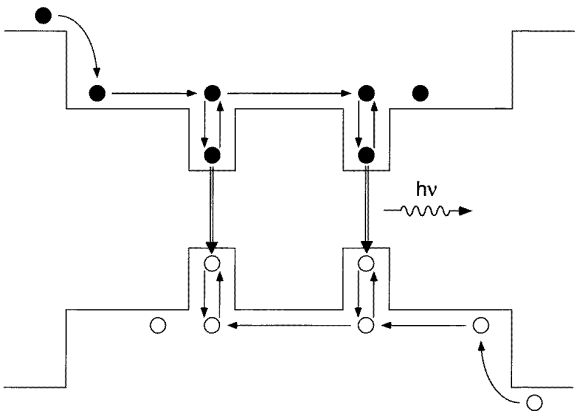

Figure 1. Interwell transport dynamics of electrical carriers in MQW optical gain media.

rate and found it to exhibit strong oscillations with the width of the QW. Specifically, they predicted a resonance enhancement in the capture rate whenever a new state is bound inside the well (and whenever a new virtual bound state, or transmission resonance, is introduced in the overlaying continuum) with eigenenergy within one LO phonon energy from the barriers band edge. In the same year and subsequently, several other calculations of the intrinsic capture lifetime were published [3–9]. In particular, the approach of [2] was extended to include the effect of hot carrier distributions [7] (which were argued to partially smear out the capture lifetime resonances) and the quantization of the LO phonon modes in the QW potential [6] (leading to additional resonances in the well width dependence). Furthermore, additional contributions to the intrinsic capture rate, other than LO phonon emission, were considered, such as impurity scattering [7] and carrier–carrier scattering [8, 9] (with the latter expected to become particularly important in the presence of the large carrier densities typical of laser operation).

On the experimental side, several different techniques have been employed to measure τ_{cap} in MQW structures based on the AlGaAs or the InGaAsP material systems, under a wide range of experimental conditions (e.g. at different temperatures, carrier densities, well and barrier widths, etc). These include static [10, 11, 38] and time-resolved [7, 12–19] photoluminescence, pump-probe spectroscopy [20–22] and modulation response measurements [23–26]. The estimated values for the capture lifetime reported in these works vary over a wide range, from several hundreds of femtoseconds to several tens of picoseconds, which is only partly justified by the differences among the samples studied. The additional complication is that typically additional transport processes other than the intrinsic capture enter in the measured time constant, to a degree dependent on the details of the experiment. This makes it quite difficult to compare the different measurements and draw some unified conclusion from them, although there is a general tendency to agree on a value of around 1 ps for the room-temperature intrinsic capture lifetime.

Regarding the QW width dependence, weak oscillations have been reported in some works [10, 18, 21]. A common feature of these experiments is that they were performed

at relatively low carrier densities, where the assumption that the unbound states are Bloch waves extended over the entire separate confinement region (implicit in all the model calculations predicting these oscillations) is more justified. On the other hand, it has been pointed out [20] that at high carrier densities carrier–carrier scattering causes a large lifetime broadening, and hence a strong reduction in the coherence length of the unbound carriers, so that they behave more like semiclassical wavepackets. Therefore, in this regime quantum effects such as the well width oscillations are expected to be washed out; some experimental results [17, 20], performed under conditions comparable with those of laser operation, seem to confirm these arguments.

Finally, it should be mentioned that, following the recent advances in the fabrication of one- and zero-dimensional semiconductor quantum structures, the capture problem in these structures has also been recently considered. In particular, it has been suggested [39] that phonon-assisted capture becomes increasingly inefficient as the dimensionality is reduced; on the other hand, Coulomb scattering becomes the dominant relaxation mechanism [40, 41]. In any case, a recent experimental investigation [42] has found a significantly reduced capture rate in quantum-dot laser structures relative to QW devices.

2.2. Implications for high-speed lasers

In the early stages of their development, QW lasers were predicted [43] to have a significantly larger direct modulation bandwidth than their bulk counterparts, mainly because of their larger differential gain. However, it was subsequently observed that the mere use of QW active layers did not result in an automatic increase in modulation bandwidth; furthermore, QW lasers were found [44, 45] to be characterized by an anomalously large, structure-dependent damping rate. These findings were eventually explained [27, 28] as resulting from carrier transport effects. In particular, in [27] it was argued that the finite overall capture lifetime gives rise to an additional contribution to the nonlinear gain compression, which is in turn responsible for the reduced modulation bandwidth. Using a similar rate equation approach, Nagarajan *et al* showed [28] that the same transport effects could instead be modelled with a reduced effective differential gain.

In any case, these early works compounded all the relevant transport processes into a single effective time constant, which they argued was dominated by the slowest process, i.e. transport across the barrier region (which, under the near-flat-band conditions typical of laser operation, is mainly due to diffusion). However, with the explicit inclusion of diffusion (and drift) in the carrier density rate equations, it was later shown [29, 30] that in general the modulation bandwidth of QW lasers is limited by the combined effect of these real-space transport processes and of the intrinsic capture (despite the fact that the latter is a much faster process). In particular, in this analysis the intrinsic capture lifetime was found to enter the laser dynamics rescaled by the factor V_{SCH}/V_{QW}, the volume ratio of the separate confinement heterostructure to the QWs (which can be large enough to make it comparable with the diffusion time). Either process may then dominate in a specific laser structure depending on the details of the active region; for instance, Nagarajan *et al* provided evidence of diffusion-limited transport in one device [31] by showing that the modulation response is limited by the holes (for which diffusion is slower and intrinsic capture faster than for the electrons). However, other experimental results [24] were successfully interpreted on the basis of the quantum capture model.

Several other theoretical models [32–36] with varying degrees of complexity have been subsequently published, including Monte Carlo simulations [35, 36]. In particular, in dealing with laser structures consisting of several QWs, it has been pointed out [32] that efficient interwell coupling is also important, since optimum operation requires good inversion of all QWs. The transport of carriers between adjacent QWs in a typical laser structure is mainly limited by the escape time from the QWs τ_{esc} (via thermionic emission), so that this time constant should not be too slow (on the other hand, τ_{esc} should be larger than τ_{cap}, or else the carriers would no longer be effectively captured in the wells).

Since this extensive body of theoretical work is focused on the frequency response of (M)QW lasers, it became natural to investigate the capture problem in (M)QW active layers (and its relevance to laser dynamics) using frequency-domain techniques. In particular, the works mentioned above [23, 24, 31] investigated the presence of transport effects in the overall modulation response of these devices. The main limitation of this approach is that the maximum modulation frequency is limited to a few tens of gigahertz at most, corresponding to a time resolution of around 10 ps or worse; therefore it cannot be used to directly study the fastest component of the capture dynamics, i.e. intrinsic capture. In the following section, we will describe how this limitation can be overcome by generating the modulation via photomixing of two nondegenerate waves, and we will then describe two applications of this technique [25, 26].

3. Carrier transport dynamics studied by four-wave mixing

The study of carrier dynamics from modulation response measurements in semiconductor lasers is complicated because the overall frequency response of these devices is affected by several contributions (including package and chip parasitics), which together set the upper limit to the modulation bandwidth. An effective technique to isolate the intrinsic response is active-layer photomixing [46], in which two external continuous waves are coupled in the laser active region, where their beating generates a carrier density modulation at their detuning frequency.

To further isolate the carrier dynamics contribution, the same approach has subsequently been applied to semiconductor optical amplifiers (SOAs) [47], i.e. semiconductor laser chips with antireflection coatings applied on both facets to minimize the optical feedback, which eliminate cavity effects from the frequency response (in particular, the double pole at the cavity complex resonance frequency is correspondingly replaced by a single pole at the inverse carrier lifetime). This technique (commonly referred to as four-wave mixing

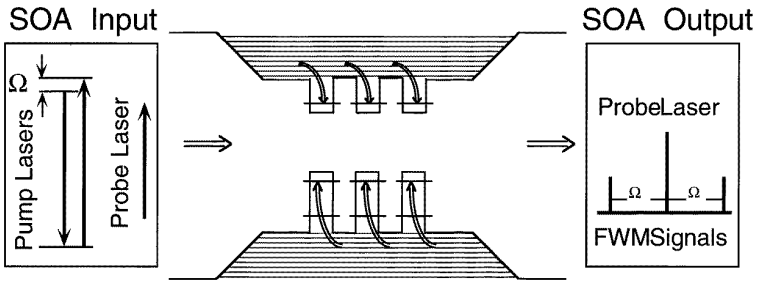

Figure 2. Schematics of the capture lifetime measurement. In this experiment, a carrier density modulation is generated in the barrier region through beating of two 1.3 μm pump waves. A fraction of this modulation is captured into the QW bound states, where it then partially scatters a 1.5 μm probe wave into two FWM sidebands.

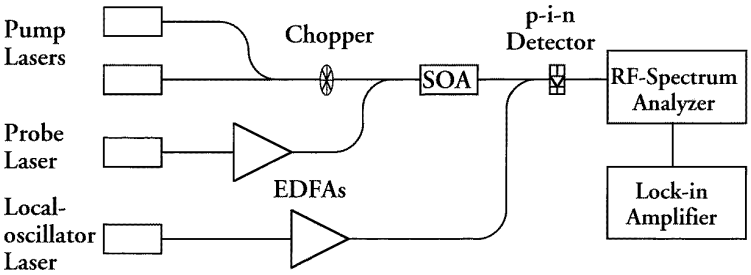

Figure 3. Experimental setup for the capture lifetime measurement.

(FWM) spectroscopy, since the modulation sidebands are generated through the FWM nonlinear interaction between the two input waves) allows the detuning frequency to be extended to several terahertz (in which case optical heterodyning is required for detection). As a result, it is well suited [47] to study of the ultrafast intraband carrier dynamics associated with optical nonlinearities such as carrier heating and spectral hole burning. It is interesting to point out that FWM can be viewed as the frequency-domain counterpart of pump-probe spectroscopy, which has also been applied to SOAs [22, 48]: specifically, while pump-probe experiments measure an impulse response function, FWM gives the corresponding frequency response.

3.1. Measurement of the intrinsic capture lifetime

As illustrated schematically in figure 2, a wavelength-resolved FWM configuration can be designed to directly study the intrinsic capture process. The basic idea behind this experiment [26] is to generate a carrier density modulation in the barrier states and probe for the presence of such a modulation inside the QWs. To this purpose, three continuous waves are coupled into the SOA waveguide: two pump waves with frequencies matching the barriers' bandgap (in the 1.3 μm band), and one probe wave with frequency near the gain peak of the SOA (in the 1.5 μm band). The beating of the two pump waves generates a modulation of the carrier density in the barrier region, at their difference frequency Ω. A fraction of this modulation is captured into the QWs where it then acts to scatter energy from the probe laser beam into two FWM sidebands. Information on the carrier capture process can then be inferred from the relative intensity of either FWM signal as a function of the modulation frequency Ω. In particular, we expect the FWM conversion efficiency to become negligibly small at modulation frequencies much larger than the capture rate (at these frequencies, the probability of the modulated carrier distribution being captured into the QWs within a few modulation periods becomes negligibly small).

It is important to emphasize that in the experiment the photon energy of the pump waves (approximately 0.94 eV) is very close to (actually slightly lower than) the barriers' bandgap energy (nominally 0.97 eV): accounting for thermal broadening, we conclude that the electronic states directly modulated by these waves are not bound in any QW (i.e. they are purely 3D states), although their wavefunctions are somewhat localized near the wells. As a result, in this experiment the limiting rate is that of the intrinsic, 'quantum' capture, fully isolated from all other transport effects. Furthermore, the use of photomixing to generate the carrier density modulation, and of a optical heterodyne system to detect the modulation sidebands on the probe wave, allows us to extend the measured bandwidth to a few hundreds of gigahertz, i.e. well beyond such intrinsic capture rates, which can then be measured directly. Incidentally, a similar technique has been used to study capture in a QW laser in [24], where the carrier density modulation was produced by injection of a directly modulated beam from another semiconductor laser; in that work, however, the modulation frequency was limited by the bandwidth of the laser source and the detection electronics to around 20 GHz, so that the intrinsic capture could not be directly isolated from the other transport processes.

The physical layout of the experiment is shown in figure 3. The input waves are provided by three temperature-tunable DFB lasers. The structure studied in this experiment is an MQW InGaAs/InGaAsP SOA (780 μm long, biased with a direct current of 100 mA), consisting of three pairs

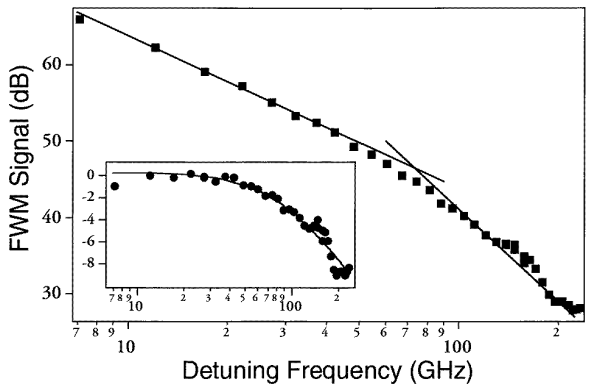

Figure 4. Results of the capture lifetime measurement: FWM signal power versus modulation frequency (the origin of the vertical axis is arbitrary). As emphasized by the continuous lines, the slope of the data changes from −20 to −40 dB/decade with increasing detuning frequency. The inset displays the same data with the initial 20 dB/decade roll-off subtracted out; the continuous curve is a single-pole frequency response with pole at 88 GHz $= 1/(2\pi \times 1.8$ ps).

of tensile and compressively strained QWs [49] (notice, however, that the presence of strain is not essential to this experiment). Approximately 17 mW of probe power (after preamplification in a high-gain erbium-doped fibre amplifier (EDFA)) and 2 mW of pump power are coupled into the device. The probe wave is linearly polarized along the TM axis of the SOA waveguide, so that only the tensile wells are probed (compressively strained QWs have negligible gain for TM light); this avoids any complication arising from possibly having different capture rates in the two types of wells. The SOA output is combined with a tunable optical local oscillator, and the beat signal between the local oscillator and either FWM sideband is detected at a constant frequency in a radio-frequency spectrum analyser. In order to increase the signal-to-noise ratio, the analogue output of the spectrum analyser is fed to a lock-in amplifier (locked to a chopper placed in the optical path of the pump waves), where the signal is measured.

A typical trace is shown in figure 4, which gives the frequency-upconverted FWM sideband with the modulation frequency ranging from 7 to 230 GHz. As emphasized by the continuous lines, the data exhibit a 20 dB/decade roll-off at low modulation frequencies and a 40 dB/decade roll-off at modulation frequencies exceeding about 90 GHz. The former roll-off is associated with the interband stimulated recombination of the carriers in the QWs (occurring at a rate $1/2\pi\tau_s$ of approximately 1.2 GHz under the present experimental condition [50]). Since the emphasis here is on the features related to the capture process, this initial roll-off was normalized out (notice that the exact value of $1/2\pi\tau_s$ used in this normalization is irrelevant, provided that it is smaller than the smallest modulation frequency measured). The result is shown in the inset of figure 4, which clearly suggests the presence of another pole at 88 GHz (corresponding to a lifetime of 1.8 ps). Additional structures are observed at larger modulation frequencies. The same features were observed in the frequency-downconverted data.

A two-pole frequency response is consistent with a model of the capture dynamics based on the following set of rate equations (in the frequency domain):

$$-\mathrm{i}\Omega N_{2D}^{(\Omega)} = -\left(\frac{1}{\tau_s}+\frac{1}{\tau_{esc}}\right)N_{2D}^{(\Omega)}+\frac{N_{3D}^{(\Omega)}}{\tau_{cap}}$$

$$-\mathrm{i}\Omega N_{3D}^{(\Omega)} = -\left(\frac{1}{\tau_s}+\frac{1}{\tau_{cap}}\right)N_{3D}^{(\Omega)}+\frac{N_{2D}^{(\Omega)}}{\tau_{esc}}+g_{3D}^{(\Omega)}. \qquad (1)$$

Here $N_{2D}^{(\Omega)}$ denotes the small-signal density of carriers confined inside each (tensile) well; $N_{3D}^{(\Omega)}$ is the density of unbound carriers localized near the same QW (and directly modulated by the beating of the pump waves, at a rate $g_{3D}^{(\Omega)}$); τ_{cap} and τ_{esc} are the intrinsic capture and escape lifetimes. Notice that we are not including in this model any effect related to transport in real space, such as diffusion or drift, as appropriate for excitation near the barriers' band edges. Furthermore, we do not explicitly consider the capture of both electrons and holes, since the frequency response measured in this experiment should be dominated by the slower carrier type (presumably the electrons [14]).

The field amplitude of either FWM sideband, as a function of the modulation frequency Ω, is proportional to the amplitude of the carrier density modulation that generates it, $N_{2D}^{(\Omega)}$. Solving the coupled set of equations (1), one finds

$$N_{2D}^{(\Omega)} = \frac{1/\tau_{cap}}{(-\mathrm{i}\Omega+1/\tau_s)(-\mathrm{i}\Omega+1/\tau_{cap}+1/\tau_{esc}+1/\tau_s)}g_{3D}^{(\Omega)} \qquad (2)$$

so that on the basis of this simple model we expect the FWM conversion efficiency to exhibit one pole at $1/\tau_s$ and another at $1/\tau_{cap}+1/\tau_{esc}+1/\tau_s$ ($\approx 1/\tau_{cap}$ since in general the capture lifetime is shorter than both the stimulated recombination and the escape lifetimes [25, 29]). Therefore, if we assume that the measured frequency dependence is entirely ascribed to the carrier density modulation response of equation (2), we obtain from figure 4 an estimate of 1.8 ps for the electronic capture lifetime.

We emphasize that a particularly attractive feature of this technique is that τ_{cap} is immediately read off the experimental data, without any involved numerical fit. This should make it quite appealing for instance to quickly compare the effectiveness of the intrinsic capture process in different (M)QW structures. Furthermore, by varying the frequency of the pump waves relative to the barriers' bandgap one should be able to observe the transition to a regime where other transport processes, in addition to intrinsic capture, begin to limit the frequency response. Finally, it should be pointed out that there are structures in the data of figure 4 (the two shoulders around 140 and 200 GHz) that are not consistent with the two-pole frequency response of equation (2), which may be a signature of additional dynamic effects in the capture process, or which may be due to wave propagation effects such as phase matching (in the latter case, which, however, is not consistent with the large absorption experienced by the pump waves in the SOAs, the above-mentioned estimate of 1.8 ps should be regarded as an upper limit to the capture lifetime). Further experimental work will allow these issues to be clarified.

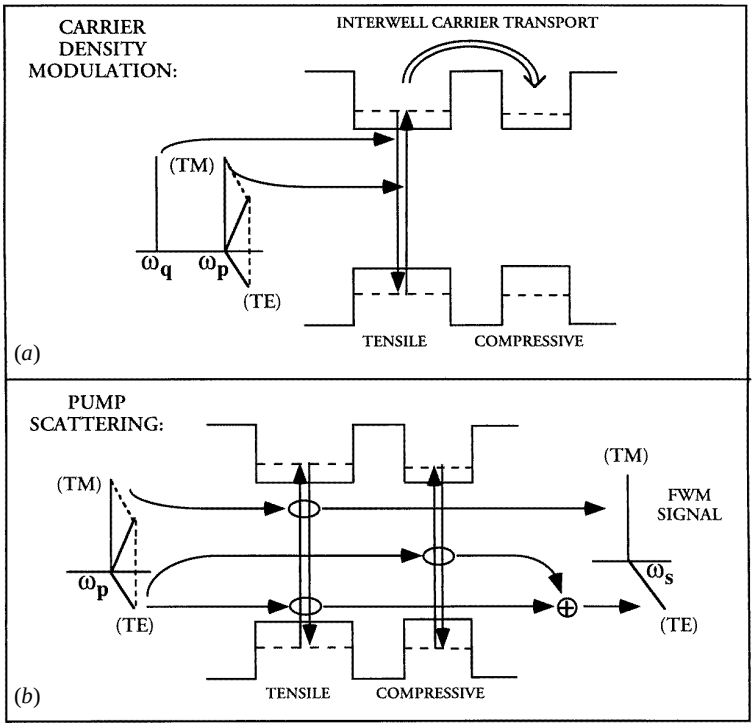

Figure 5. Schematics of the FWM processes taking place with the polarizations used in the interwell transport lifetime measurement. As shown in (*a*), modulation of the carrier density is generated directly (through beating of the TM components of the input waves) only in the tensile wells, from which it can then be transferred to the neighbouring compressive wells. Each polarization component of the pump is then correspondingly scattered into the same component of the FWM signal as shown in (*b*).

3.2. Measurement of the interwell equilibration lifetime

In this section we will describe another frequency-domain experiment [25], based on polarization-resolved FWM in a specially designed SOA, aimed at studying the process of interwell equilibration. The basic idea, similar in principle to that of the capture lifetime measurement just described, is to create a carrier density modulation in a QW and probe for the presence of such a modulation in a neighbouring well. The strength of the corresponding modulation sidebands (FWM signals) strongly depends on the interwell transport rate (which will be denoted by $1/\tau_t$); in particular, we expect it to become negligibly small at modulation frequencies much larger than this rate. As a result, FWM can be used to measure τ_t, provided that the contribution to the overall FWM signal involving interwell transport can somehow be isolated from all other contributions. As will be shown below, this can be done by taking advantage of the FWM polarization selection rules in an alternating-strain SOA. This technique then provides a direct way of studying interwell transport, which, as discussed in section 2, is another issue of considerable importance regarding the modulation properties of MQW lasers.

The FWM polarization configuration used in this work is illustrated in figure 5. The SOA (the same device used in the measurement of section 3.1) consists of three alternating pairs of a tensile and a compressively strained QW and was designed for polarization-independent small-signal gain [49] (the crucial feature in this context is the negligibly small optical gain provided by compressive wells to TM polarized waves). Coupled into this device are a probe wave linearly polarized along the growth axis (TM polarization) and a pump wave with equal TE and TM components. With this choice for the input polarization states, a carrier density modulation can only be generated by beating of the TM components of the pump and probe waves, which can only occur in the tensile wells (since, as was just mentioned, compressive wells have no gain for TM-polarized light). Here, each polarization component of the pump wave is then partially scattered by this modulation to generate a FWM sideband with equal polarization. Furthermore, if the carrier density modulation is efficiently transferred into the neighbouring compressive wells, an additional contribution to the TE component of the FWM signal can be generated there. We notice that the use of polarization to discriminate between the contributions from tensile and compressive wells in alternating-strain SOAs has been originally demonstrated in a FWM experiment in [51], and it has also been subsequently employed in a time-domain pump-probe experiment [22].

Figure 5(*b*) gives a schematic representation of the different processes contributing to the FWM signal field $\boldsymbol{E}^{(s)}$, which can accordingly be written as

$$E_1^{(s)} = (\chi_{12}^T + \chi_{12}^{C\leftarrow T})(E^{(p)})^2(E^{(q)})^*$$

$$E_2^{(s)} = \chi_{22}^T(E^{(p)})^2(E^{(q)})^*. \qquad (3)$$

In these expressions, χ_{il} is the complex amplitude for scattering of the ith component of the pump by a modulation

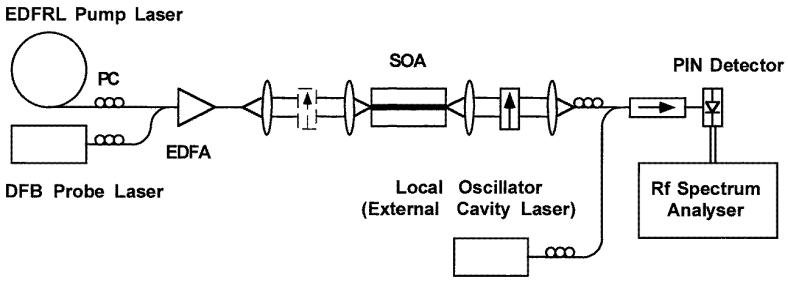

Figure 6. Experimental setup for the interwell transport lifetime measurement.

generated through beating of the lth components of the two input waves; the subscripts $i = 1, 2$ denote the TE and TM directions respectively; $\boldsymbol{E}^{(q)} = \hat{e}_2 E^{(q)}$ and $\boldsymbol{E}^{(p)} = (\hat{e}_1 + \hat{e}_2)E^{(p)}$ are the vector fields of the probe and the pump wave, respectively. Finally, the superscripts T and C are used to distinguish between quantities in the tensile and compressive wells, and the term proportional to $\chi_{12}^{C\leftarrow T}$ describes the contribution involving interwell transport. Information about the interwell coupling is then obtained by plotting $P_1^s/P_2^s = |(\chi_{12}^T + \chi_{12}^{C\leftarrow T})/\chi_{22}^T|^2$ (P_i^s denoting the optical power in the ith component of the FWM signal) versus modulation frequency Ω. In particular, this curve is expected to approach a constant value (proportional to $|\chi_{12}^T/\chi_{22}^T|^2$) for Ω much larger than $1/\tau_t$ (in which case the interwell transfer becomes ineffective). Any feature observed at lower modulation frequencies can vice versa be ascribed to interwell coupling.

The experimental setup used to carry out this measurement is shown in figure 6. The pump wave (provided by a tunable erbium-doped fibre ring laser (EDFRL)) and the probe (provided by a commercial DFB laser) are combined in a fibre bidirectional coupler, amplified in a high-power EDFA and then coupled into the SOA. The desired polarization states at the input of the SOA are obtained with two polarization controllers (PCs) immediately following the two lasers. At the output of the SOA a linear polarization filter is used to select the TE or the TM component of the FWM signal, which is then detected using an optical heterodyne system.

The results are shown in figure 7, where we plot the measured optical power in the TE and TM components of the FWM signal (figure 7(*a*)) and their ratio (figure 7(*b*)). These data are consistent with the previous discussion: in particular, the ratio approaches a constant at the larger values of Ω, while for Ω smaller than approximately 40 GHz an obvious deviation from this constant value is observed, which we regard as a signature of interwell coupling. Furthermore, based on this interpretation, from the data we can directly obtain an upper limit to the interwell equilibration rate $1/2\pi\tau_t$, 40 GHz in this device.

For more quantitative results, we fit the experimental data of figure 7 to a rate equation model similar to the one discussed in the previous section. In particular, equations (1) still apply, except that two distinct sets of such equations are required for the two types of wells, and furthermore in this case the modulation is directly applied to the carriers bound in the tensile wells (hence a modulation rate, which will be denoted by $g_{2D}^{T(\Omega)}$, is introduced in the rate equation for $N_{2D}^{T(\Omega)}$,

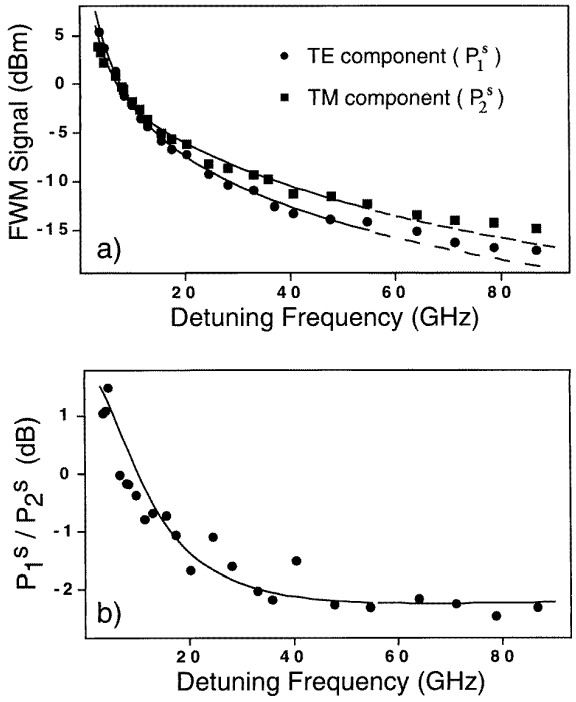

Figure 7. Results of the interwell transport lifetime measurement: (*a*) TE (circles) and TM (squares) components of the FWM signal and (*b*) their ratio versus detuning frequency. The continuous lines are fits to the theory discussed in the text. As emphasized by the broken lines, the fit becomes inaccurate in (*a*) for $\Omega >$ about 50 GHz, where carrier heating, not included in the fit, becomes important (however, since this contribution is approximately the same for the TE and TM components, the fit remains good for their ratio in (*b*)). An approximate transport lifetime of 16 ps is inferred from the data.

while $g_{3D}^{(\Omega)} = 0$ here). The interwell transport dynamics is then included in the model by writing the appropriate equation of motion for the density of unconfined electrons as a function of position along the growth axis. We point out from the outset that tunnelling will be neglected in this analysis, which is a fair assumption given the relatively large barrier width L_b (125 Å) in the SOA under study (incidentally, when the interwell coupling is dominated by resonant tunnelling, a polarization-resolved FWM excitation similar to the one described here can be used to generate a steady-state electric dipole oscillation across the barrier, as discussed theoretically in [52]). Interwell transport is then entirely ascribed to the combination of escape from a QW, drift–diffusion across the

barriers and capture in a neighbouring well. Furthermore, as before we do not consider explicitly the dynamics of holes, which are known to a have a shorter capture lifetime [14].

Regardless of the details of the boundary-value problem used to model the dynamics of the unbound carriers, its solution can be used to eliminate the variables $N_{3D}^{T(\Omega)}$ and $N_{3D}^{C(\Omega)}$ from the carrier density rate equations and recast them in the following form:

$$-\mathrm{i}\Omega N_{2D}^{T(\Omega)} = -\frac{N_{2D}^{T(\Omega)}}{\tau_e^T} + \frac{N_{2D}^{C(\Omega)}}{\tau_t^{T\leftarrow C}} + g_{2D}^{T(\Omega)}$$

$$-\mathrm{i}\Omega N_{2D}^{C(\Omega)} = -\frac{N_{2D}^{C(\Omega)}}{\tau_e^C} + \frac{N_{2D}^{T(\Omega)}}{\tau_t^{C\leftarrow T}} \tag{4}$$

where $1/\tau_e^T$ is an effective escape rate from the tensile wells and $1/\tau_t^{C\leftarrow T}$ is the overall transport rate from the tensile wells to the neighbouring compressive wells (or in other words $\tau_t^{C\leftarrow T}$ is the time it takes the compressive wells to equilibrate to the tensile wells in this device). In [53], we describe a detailed model of the interwell transport dynamics (in which diffusion is taken to be the dominant real-space transport process), which allows us, under a given set of simplifying assumptions, to express these rates in terms of the capture and escape lifetimes τ_{cap} and τ_{esc} (actually, in this model both $1/\tau_e$ and $1/\tau_t$ are found to be complex-valued functions of Ω, owing to their dependence on the diffusion length).

The set of equations (4) has solutions

$$N_{2D}^{T(\Omega)} = \frac{\tau_e^T(1-\mathrm{i}\Omega\tau_e^C)}{(1-\mathrm{i}\Omega\tau_e^C)(1-\mathrm{i}\Omega\tau_e^T) - \tau_e^C\tau_e^T/(\tau_t^{C\leftarrow T}\tau_t^{T\leftarrow C})} g_{2D}^{T(\Omega)}$$

$$N_{2D}^{C(\Omega)} = \frac{\tau_e^C\tau_e^T/\tau_t^{C\leftarrow T}}{(1-\mathrm{i}\Omega\tau_e^C)(1-\mathrm{i}\Omega\tau_e^T) - \tau_e^C\tau_e^T/(\tau_t^{C\leftarrow T}\tau_t^{T\leftarrow C})} g_{2D}^{T(\Omega)} \tag{5}$$

which can be used to fit the data of figure 7, given that each contribution to the FWM signal is proportional to the carrier density modulation that generates it (i.e. χ_{12}^T, $\chi_{22}^T \propto N_{2D}^{T(\Omega)}$ and $\chi_{12}^{C\leftarrow T} \propto N_{2D}^{C(\Omega)}$ in equations (3)). In carrying out this fit we neglect any difference between the time constants of the two types of wells, and furthermore we assume $\tau_e = \tau_t$ (neglecting interband recombination, the carriers that escaped from the tensile wells are eventually transported in the compressive wells and vice versa).

The continuous lines in figure 7 are the fits to the model theory just described. The agreement with the experimental data is excellent, except for the points at detuning frequencies in excess of about 50 GHz, where carrier heating (not included in the model) is known [47] to cause an increase in the FWM conversion efficiency. Note, however, that since this increase is approximately the same for both the TE and TM components, the fit remains good for their ratio in figure 7(*b*). From this fit, we obtain an estimate of 16 ps for the (low-frequency) interwell transport lifetime τ_t, as well as for τ_e. Furthermore, if we assume that τ_t and τ_e are related to the quantum capture–escape lifetimes as given by the model of [53], we find $\tau_{esc} \approx 8$ ps, and $\tau_{cap} \approx 1.5$ ps. While these estimates rely on several additional simplifying assumptions, it is worthwhile to emphasize that the estimate of τ_{cap} compares favourably with the value measured in the same SOA in the experiment described in section 3.1.

4. Conclusions

In this review, we have discussed the interwell transport dynamics of electrical carriers in semiconductor MQW structures. We have mainly considered the case of electrically pumped active layers (e.g. high carrier density regime), in which carrier transport results from the interplay between classical diffusion and drift, and quantum capture transitions. The dynamic properties of MQW diode lasers are strongly related to the effectiveness of this composite capture process, and we have briefly reviewed the large body of theoretical and experimental work aimed at exploring this relation. On the device level, of particular importance is the development of simple and reliable techniques to measure the time constants governing the different components of this dynamics.

In particular, we have described in detail two such experimental techniques, based on FWM in SOAs, and designed to directly study, in the frequency domain, the intrinsic capture process and the transfer of carriers between adjacent QWs. As illustrated by the results presented in section 3, these techniques are quite attractive because the transport processes under study appear as qualitatively new features in the measurement results (i.e. the 20 dB/decade roll-off in the normalized data shown in the inset of figure 4 and the low-frequency shoulder in the data of figure 7(*b*)). Furthermore, the 'cutoff' frequency of each of these features is a direct measure of the effectiveness of the corresponding process, which is immediately obtained from the experimental data. Finally, we have presented a rate-equation description of these experiments that can be used to fit the data and obtain, subject to a few assumptions, numerical estimates of the relevant time constants. This approach is then ready to be used for a systematic study of the carrier transport properties of different MQW active structures.

Acknowledgments

The authors would like to thank Ortel Corporation for the loan of certain components used in the experiments and Uzi Koren of Lucent Technologies for providing the SOAs. This work was supported by ARPA (Contract DAAL 01-94-K-03430) and the National Science Foundation (Grant ECS-9412862).

References

[1] Shah J 1996 *Ultrafast Spectroscopy of Semiconductors and Semiconductor Nanostructures* (Berlin: Springer)
[2] Brum J A and Bastard G 1986 *Phys. Rev.* B **33** 1420
[3] Kozyrev S V and Shik Y 1985 *Sov. Phys.–Semicond.* **19** 1024
[4] Murayama Y 1986 *Phys. Rev.* B **34** 2500
[5] Babiker M and Ridley B K 1986 *Superlattices Microstruct.* **2** 287
[6] Babiker M, Chamberlain M P and Ridley B K 1987 *Semicond. Sci. Technol.* **2** 582
[7] Deveaud B, Chomette A, Morris D and Regreny A 1993 *Solid State Commun.* **85** 367

[8] Blom P W M, Haverkort J E M, van Hall P J and Wolter J H 1993 *Appl. Phys. Lett.* **62** 1490
[9] Preisel M, Mork J and Haug H 1994 *Phys. Rev.* B **49** 14 478
[10] Ogasawara N, Fujiwara A, Ohgushi N, Fukatsu S, Shiraki Y, Katayama Y and Ito R 1990 *Phys. Rev.* B **42** 9562
[11] Tessler N, Nagar R, Abraham D, Eisenstein G, Koren U and Raybon G 1992 *Appl. Phys. Lett.* **60** 665
[12] Westland D J, Mihailovic D, Ryan J F and Scott M D 1987 *Appl. Phys. Lett.* **51** 590
[13] Polland H J, Leo K, Rother K, Ploog K, Feldmann J, Peter G, Gobel E O, Fujiwara K, Nakayama T and Otha Y 1988 *Phys. Rev.* B **38** 7635
[14] Deveaud B, Shah J, Damen T C and Tsang W T 1988 *Appl. Phys. Lett.* **52** 1886
[15] Oberli D Y, Shah J, Jewell J L, Damen T C and Chand N 1989 *Appl. Phys. Lett.* **54** 1028
[16] Morin S, Deveaud B, Clerot F, Fujiwara K and Mitsunaga K 1991 *IEEE J. Quantum Electron.* **27** 1669
[17] Kersting R, Schwedler R, Wolter K, Leo K and Kurz H 1992 *Phys. Rev.* B **46** 1639
[18] Blom P W M, Smit C, Haverkort J E M and Wolter J H 1993 *Phys. Rev.* B **47** 2072
[19] Davis L, Lam Y L, Chen Y C, Singh J and Bhattacharya P K 1994 *IEEE J. Quantum Electron.* **30** 2560
[20] Weiss S *et al* 1992 *Appl. Phys. Lett.* **60** 9
[21] Barros M R X, Becker P C, Morris D, Deveaud B, Regreny A and Beisser F 1993 *Phys. Rev.* B **47** 10 951
[22] Lenz G, Ippen E P, Wiesenfeld J M, Newkirk M A and Koren U 1996 *Appl. Phys. Lett.* **68** 2933
[23] Chung Y C, Wiesenfeld J M, Raybon G, Koren U and Twu Y 1991 *IEEE Photonics Technol. Lett.* **3** 130
[24] Vassilovski D, Wu T C, Kan S, Lau K Y and Zah C E 1995 *IEEE Photonics Technol. Lett.* **7** 706
[25] Paiella R, Hunziker G, Vahala K J and Koren U 1996 *Appl. Phys. Lett.* **69** 4142
[26] Paiella R, Hunziker G, Vahala K J and Koren U 1997 *Appl. Phys. Lett.* **71** 3601
[27] Rideout W, Sharfin W F, Koteles E S, Vassell M O and Elman B 1991 *IEEE Photonics Technol. Lett.* **3** 784
[28] Nagarajan R, Fukushima T, Corzine S W and Bowers J E 1991 *Appl. Phys. Lett.* **59** 1835
[29] Kan S C, Vassilovski D, Wu T C and Lau K Y 1992 *Appl. Phys. Lett.* **61** 752
[30] Wu T C, Kan S C, Vassilovski D and Lau K Y 1993 *Appl. Phys. Lett.* **63** 441
[31] Nagarajan R, Mirin R P, Reynolds T E and Bowers J E 1993 *Electron. Lett.* **29** 1688
[32] Tessler N and Eisenstein G 1993 *IEEE J. Quantum Electron.* **29** 1586
[33] Weisser S, Esquivias I, Tasker P J, Ralston J D, Romero B and Rosenzweig J 1994 *IEEE Photonics Technol. Lett.* **6** 1421
[34] Tsai C Y, Tsai C Y, Lo Y H, Spencer R M and Eastman L F 1995 *IEEE J. Sel. Top. Quantum Electron.* **1** 316
[35] Lam Y and Singh J 1993 *Appl. Phys. Lett.* **63** 1874
[36] Grupen M and Hess K 1998 *IEEE J. Quantum Electron.* **34** 120
[37] Shichijo H, Kolbas R M, Holonyak N, Dupuis R D and Dapkus P D 1978 *Solid State Commun.* **27** 1029
[38] Tang J Y, Hess K, Holonyak N, Coleman J J and Dapkus P D 1982 *J. Appl. Phys.* **53** 6043
[39] Benisty H, Sotomayor-Torres C M and Weisbuch C 1991 *Phys. Rev.* B **44** 10 945
[40] Bockelmann U and Egeler T 1992 *Phys. Rev.* B **46** 15 574
[41] Vurgaftman I and Singh J 1994 *Appl. Phys. Lett.* **64** 232
[42] Klotzkin D, Kamath K and Bhattacharya P 1997 *IEEE Photonics Technol. Lett.* **9** 1301
[43] Arakawa Y and Yariv A 1985 *IEEE J. Quantum Electron.* **21** 1666
[44] Sharfin W F, Schlafer J, Rideout W, Elman B, Lauer R B, LaCourse J and Crawford F D 1991 *IEEE Photonics Technol. Lett.* **3** 193
[45] Fukushima T, Bowers J E, Logan R A, Tanbun-Ek T and Temkin H 1991 *Appl. Phys. Lett.* **58** 1244
[46] Vahala K J and Newkirk M A 1989 *IEEE J. Quantum Electron.* **25** 1393
[47] Zhou J, Park N, Dawson J D, Vahala K J, Newkirk M A and Miller B I 1993 *Appl. Phys. Lett.* **63** 1179
[48] Hall K L, Mark J, Ippen E P and Eisenstein G 1990 *Appl. Phys. Lett.* **56** 1740
[49] Newkirk M A, Miller B I, Koren U, Young M G, Chien M, Jopson R M and Burrus C A 1993 *IEEE Photonics Technol. Lett.* **4** 406
[50] Hunziker G, Paiella R, Vahala K J and Koren U 1996 *IEEE Photonics Technol. Lett.* **8** 1633
[51] Zhou J, Park N, Vahala K J, Newkirk M A and Miller B I 1994 *Appl. Phys. Lett.* **65** 1897
[52] Paiella R and Vahala K J 1996 *IEEE J. Quantum Electron.* **32** 721
[53] Paiella R, Hunziker G, Koren U and Vahala K J 1997 *IEEE J. Sel. Top. Quantum Electron.* **3** 529